INTRODUCTION

While investigating a catastrophic failure of connecting rods in a medium speed four-stroke engine that occurred without any warning, a simple explanation for the problem in the form of hydrolock was proposed by several investigating parties. The rod was found to have bent before breaking into two parts. Similar cases have been reported in the past where the end result was either a bent connecting rod and/or complete failure of the connecting rod as in this case. The theory of hydro-lock has traditionally been proposed in most cases of connecting rod failures and this theory has been widely supported by engine manufacturers. In this case, a thorough investigation proved that hydrolock could not have occurred, as there is not enough energy in the engine at start to bend the rod and also there are safety devices installed on the engine to avoid ydrolock.

FIGURE 1. PICTURES OF THE FAILED CONNECTING RODS

CONNECTING ROD LOADING PARAMETERS:

The first step in analyzing the connecting rod is to define the complex state of loading to which it is exposed. A typical connecting rod from a modern diesel engine is normally subjected to the following loading.

1) The connecting rod experiences high cyclic loads, which range from high compressive loads due to the combustion gas forces and relatively high tensile loads due to the inertias. **2)** Unsymmetrical loading develops from the piston axis being out of line with the connecting rod axis.

3) The rotary vibration of the piston due to the torsional stiffness of the connecting rod. **4)** The connecting rod undergoes a very complex motion and the resulting accelerations cause lateral loads to develop, which introduce bending. The lateral and axial loads are calculated using the analytical vector approach [1]. Figure 2 shows the resulting forces calculated for the two ends of the connecting rod. Figure 3 shows the summary of loads that were calculated without considering the unsymmetrical loading.

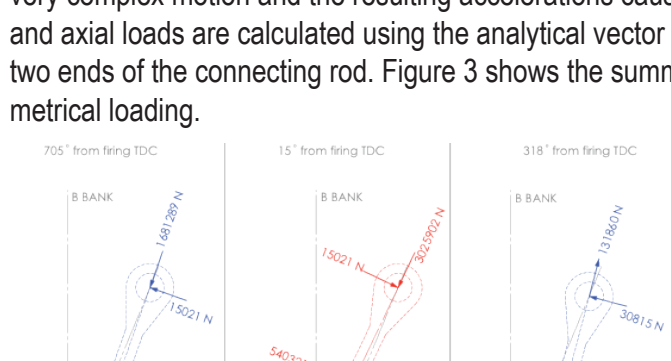

FIGURE 3. IDEAL LOAD CALCULATIONS WITHOUT UNSYMMETRICAL LOADING

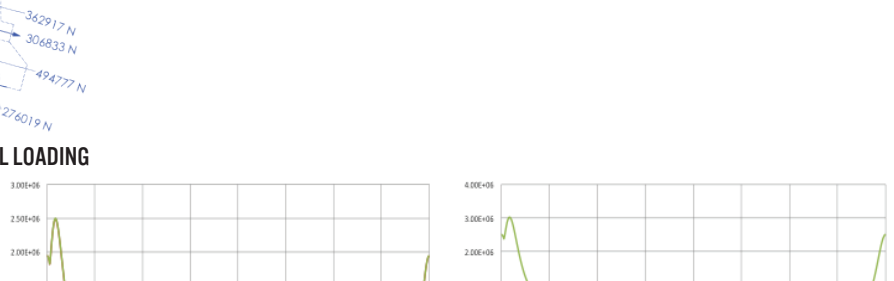

A) FORCE AT THE PISTON PIN END

B) FORCE AT THE CRANK END

FIGURE 2. FORCE AT THE TWO ENDS OF THE CONNECTING ROD

BUCKLING BEHAVIOR:

Due to the nonuniform cross-section of the connecting rod between the pin centers and its very low slenderness ratio, a nonlinear collapse analysis using the finite element method was conducted to determine the buckling behavior. Three load cases are considered; 1) compression load only, 2) compression load with lateral, torsional, and unsymmetric loads, and 3) compression load with lateral, torsional, and unsymmetric loads at reduced strength levels due to thermal and cyclic loading effects.

The finite element model shown in figure 4 a) was developed using MSC Mentat. The rod is modeled with 8-noded solid hexagonal elements having an assumed strain formulation and the piston pin and crankshaft are modeled as rigid cylinders.

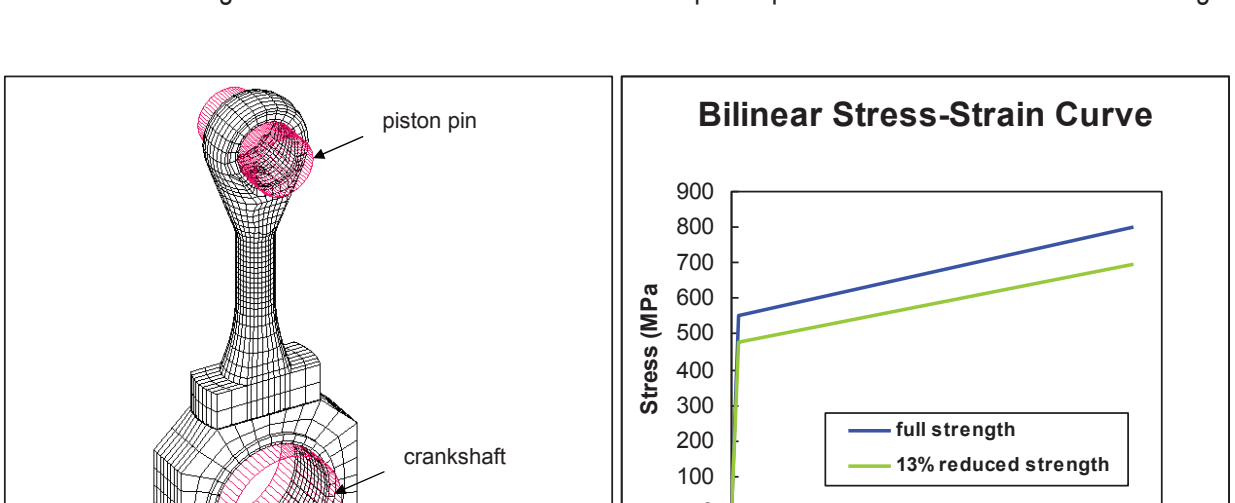

A) FINITE ELEMENT MESH B) STRESS-STRAIN CURVES

FIGURE 4. FINITE ELEMENT MESH AND STRESS-STRAIN CURVES FOR CONNECTING ROD

Contact is defined such that the rod material is free to slide relative to the rigid cylinders and represents a “pinned-pinned” connection. The rod is constrained in the axial (z) direction at the crankshaft end. The constraint condition at the piston pin end prevents the rod end from displacing in the z-direction with a 1 mm gap in either direction. The material for the connecting rod is defined in Table 1. To capture a realistic collapse phenomenon, the nonlinear material behavior must be

TABLE 1. MECHANICAL PROPERTIES AT ROOM TEMPERATURE

Component	Material	Elastic Modulus (GPa)	Poisson’s Ratio	Yield Strength (MPa)	Ultimate Strength (MPa)	Elongation %
Connecting rod	Steel	207	0.3	550	800	14

included. The connecting rod has a maximum operating temperature of 85°C (185°F). At the elevated temperature the compressive yield strength of the connecting rod material is reduced by 8%[2].

Data exists that the compressive yield strength is further reduced when exposed to cyclic loads[3]. A conservative estimate for this effect is 5%. Therefore an overall estimate of the combined reduction in the compressive yield strength of the connecting rod, during engine operation, is estimated at 13%. Using these strength reductions on a full strength curve (Blue curve) and the strengths listed in table 1, the 13% reduced strength bilinear stress-strain curve (Green curve) shown in figure 4 b) was developed. Note that these are conservative estimates based on similar materials and should be verified with testing of the actual connecting rod material.

A nonlinear material and large displacement finite element analysis was conducted using MSC.MARC. For load case 1),

the rigid pin cylinder is loaded collinearly with the center axis of the connecting rod to and beyond the critical collapse load. For load case 2 and load case 3, the connecting rod is preloaded with inertial loads and moments in the first load step, followed by a second load step that includes the same compressive load on the rigid pin as in load case 1. The resulting force-displacement curves for all three load cases are shown in figure 5. The collapse mode associated with load case 1 is an S-shape mode as shown in figure 6 a) and the collapse mode associated with load case 2 and load case 3 is a C-shape as shown in figure 6 b). The C-shape buckling mode in the connecting rod occurs when a lateral load exists and is sufficiently high enough to create a differential distance between the line of the applied compressive load and the central axis of the connecting rod. When this occurs, an additional moment is created that leads to material yielding followed by immediate collapse of the rod in a C-shape. The S-shape buckling mode occurs when there is an insufficient lateral load to initiate the C-shape buckling mode. Instead, a greater load is required to initiate yielding of the rod. Without the eccentric loading previously described for the C-shape buckling mode, the yielding continues with increasing load and the rod compresses plastically in the axial direction. Eventually, due to minute variations in the material and/or geometry, a shear plane develops as in classical compression failures.

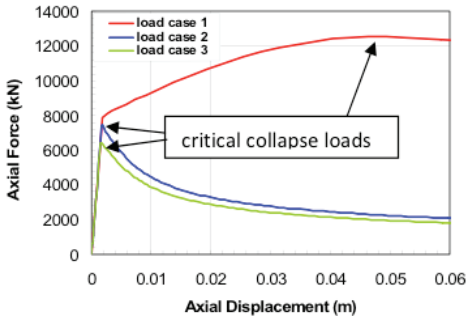

FIGURE 5. AXIAL FORCE-AXIAL DISPLACEMENT RESPONSE OF CONNECTING ROD

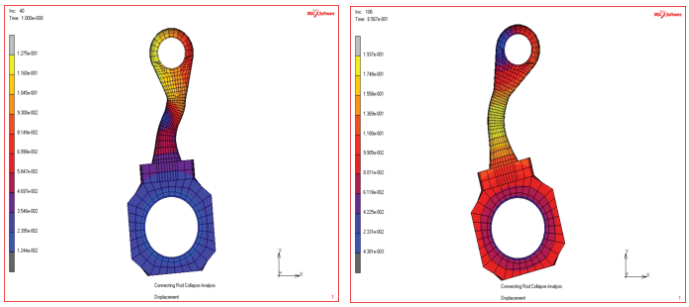

A) LOAD CASE 1 B) LOAD CASES 2 AND 3

FIGURE 6. COLLAPSE MODES

CONNECTING ROD VIBRATION (MODAL) ANALYSIS:

The critical buckling loads observed in figure 6 are more than twice what the connecting rod experiences during normal operating conditions and therefore are not sufficient to explain the observed buckling failures. The dynamic interaction failure theory hypothesizes that a crankshaft torsional mode is resonant with the connecting rod lateral vibration mode and can increase the lateral loading to a critical level. To explore this, the dynamics of the connecting rod and crankshaft needs to be defined. A modal analysis was conducted using the finite element model shown in figure 4 a). The first mode shape is the C-shape mode as shown in figure 7 with a natural frequency of 118Hz without any prestress and with a natural frequency of 114Hz when it is prestressed to the operating axial combustion loads. As was observed in the collapse analysis for load cases 2 and 3, the connecting rod will collapse upon the onset of nonlinear behavior when the material begins to yield. Therefore, the critical lateral load required to produce yielding in combination with the normal operating combustion load must be determined. The associated peak deflection of the connecting rod is then used as a criterion for its frequency response to the resonant excitation of the crankshaft. Figure 8 shows the location of the material yielding onset and the associated peak lateral deflection.

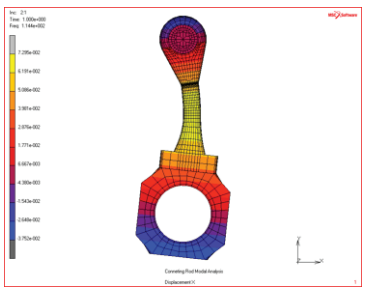

FIGURE 7. 1ST MODE SHAPE OF CONNECTING ROD

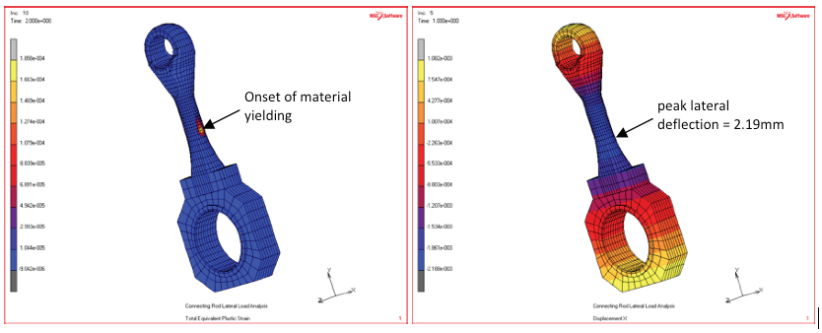

A) ONSET OF MATERIAL YIELDING B) ASSOCIATED DEFLECTION

FIGURE 8. RESPONSE TO CRITICAL LATERAL LOAD

TORSIONAL VIBRATION ANALYSIS:

A torsional vibration analysis of the diesel engine-generator system is used to determine its modal (natural) frequencies for the various mode shapes. The following mass elastic system shown in figure 9 was used for the torsional vibration analysis. The results show that there is a frequency of 113.3 Hz (7th mode of vibration) close to the engine operating speed of 514 RPM. This crankshaft natural frequency was found to cause resonance with the 1st mode of connecting rod natural frequency of 114 Hz. Figure 10 below shows the calculated tangential turning moment of the crankshaft in the time domain. Figure 11 and figure 12 show the Fourier transform of the time signal in the frequency domain.

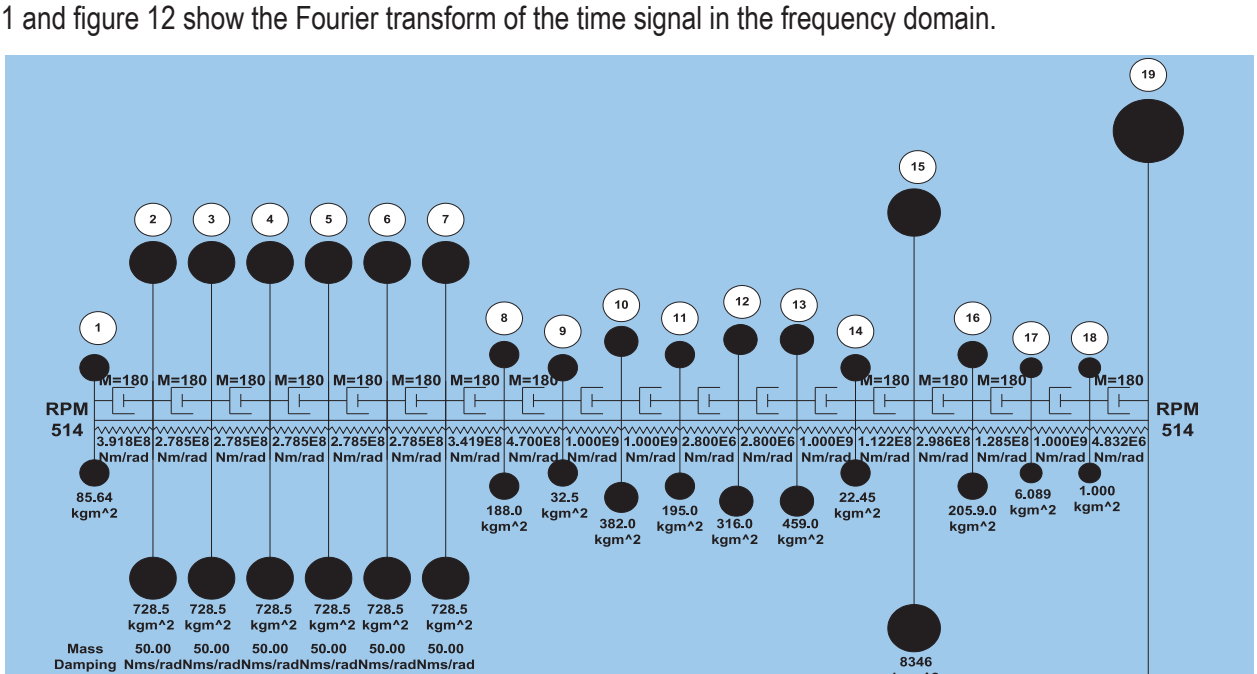

FIGURE 9. MASS-ELASTIC SYSTEM

EXCITATION FROM THE CRANKSHAFT:

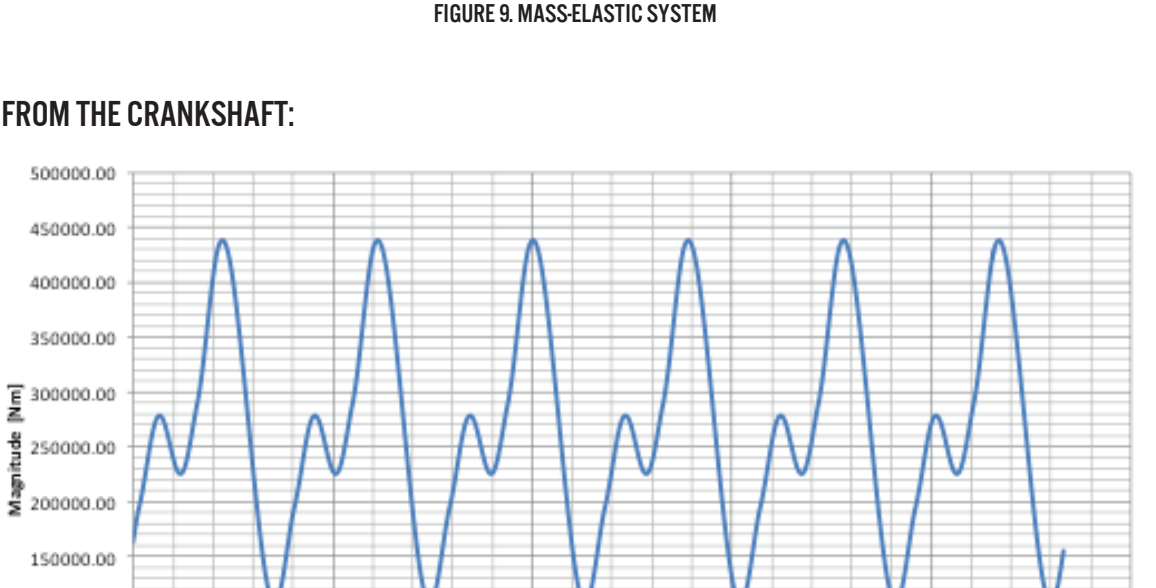

FIGURE 10. RESULTANT TANGENTIAL TURNING MOMENT IN THE TIME DOMAIN

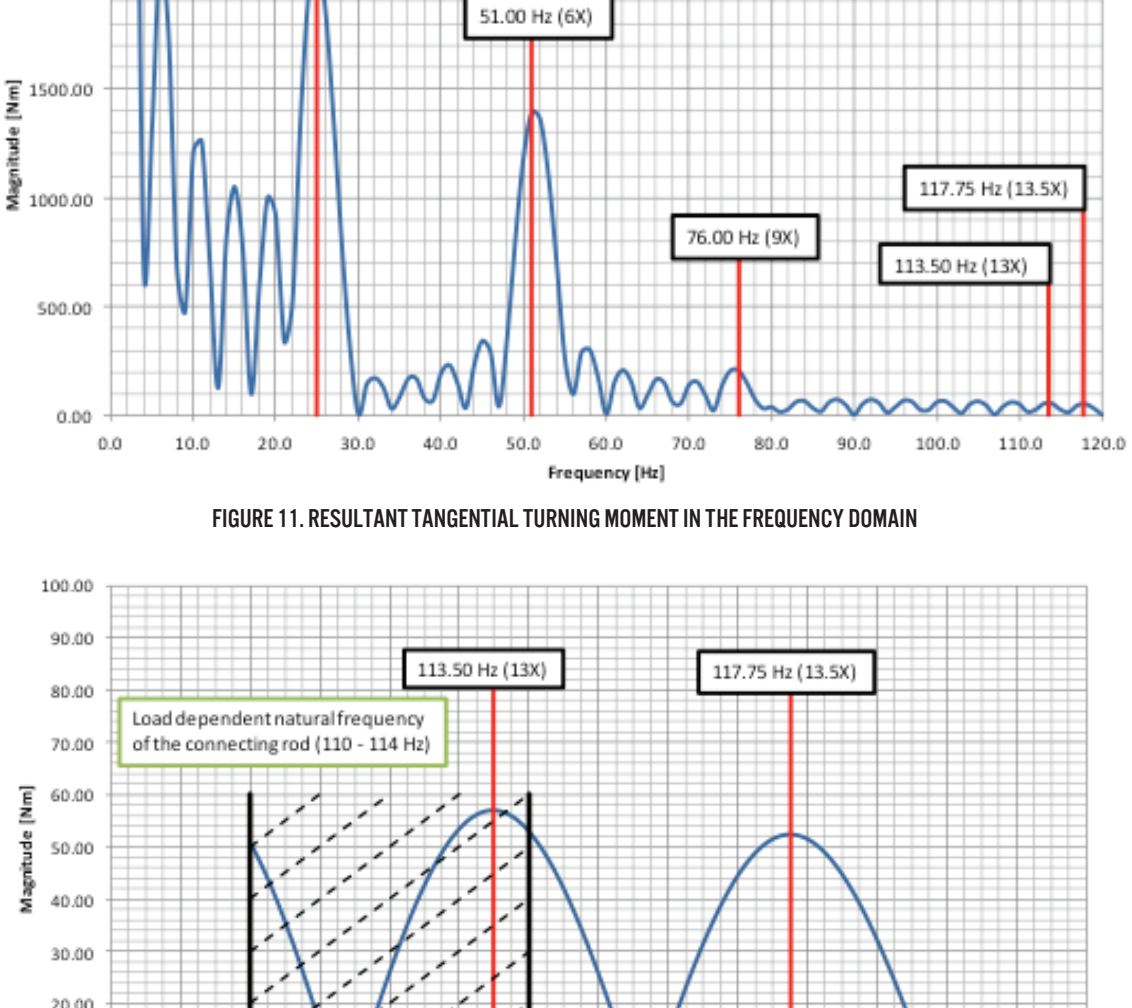

FIGURE 11. RESULTANT TANGENTIAL TURNING MOMENT IN THE FREQUENCY DOMAIN

FIGURE 12. LOAD DEPENDENT NATURAL FREQUENCY OF CONNECTING ROD OCCURS CLOSE TO 13TH ENGINE ORDER

The motion of the crankshaft is enforced as a time dependent boundary condition. Since this is a direct transient dynamic analysis, the RPM of the crankshaft cannot be instantaneously applied, as it will generate artificially excessive loads. Instead, the motion of the crankshaft must be gradually ramped up to its steady state. The following boundary conditions must be satisfied;

At time = 0.0 sec;

$$\theta = 0.0$$

$$\frac{d\theta}{dt} = 0.0$$

$$\frac{d^2\theta}{dt^2} = 0.0$$

time = t1 sec;

$$\theta = 2\pi$$

$$\frac{d\theta}{dt} = \omega$$

$$\frac{d^2\theta}{dt^2} = 0.0$$

where θ is the angle of rotation for the crankshaft, ω is the steady-state operating angular velocity of the crankshaft (514 RPM = 53.83rad/sec). A fifth order polynomial is chosen to satisfy these conditions as,

$$\theta = At^5 + Bt^4 + Ct^3 + Dt^2 + Et + F$$

Combing this equation with the above boundary conditions and solving for the polynomial coefficients produces the start up motion of the crankshaft to be defined as,

$$\theta = At^5 + Bt^4 + Ct^3$$

where, $A = \frac{12\pi}{t_1^5} - \frac{3\omega}{t_1^4}$; $B = -\frac{5}{2}At_1 - \frac{\omega}{2t_1^3}$; $C = -\frac{10}{3}At_1^2 - 2Bt_1$

The preferred motion for the finite element analysis is in the Cartesian coordinate system where the motion in the x- and y-directions are defined respectively as,

$$u = r\,\mathbf{sin}(\theta)$$
$$v = r(1 - \mathbf{cos}(\theta))$$

and differentiating with respect to time yields the Cartesian velocities,

$$\frac{du}{dt} = r\,\mathbf{cos}(\theta)\frac{d\theta}{dt}$$
$$\frac{dv}{dt} = r\,\mathbf{sin}(\theta)\frac{d\theta}{dt}$$

where r is the radial distance of the crankshaft pin center to the crankshaft's rotational axis. The resulting motions are plotted in figure 13, where the Cartesian velocity units are meters/sec.

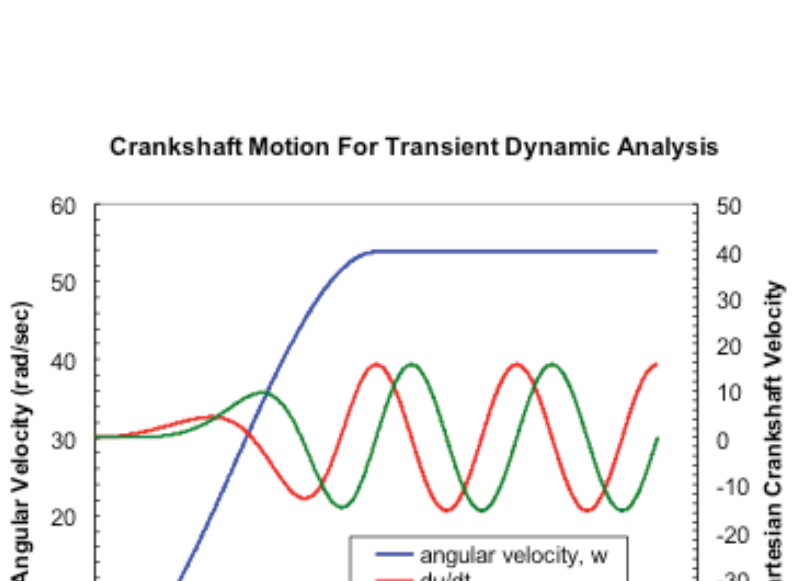

FIGURE 13. CRANKSHAFT MOTION USED TO DRIVE CONNECTING ROD

ANALYSIS OF THE DYNAMIC INTERACTION

The frequency response of the connecting rod to the excitation of the crankshaft is analyzed using a direct integration frequency response finite element analysis. For this phase of the analysis, all loads are replaced with a single harmonic input as illustrated in figure 14 a), where the acceleration amplitude A is to be determined such that the resulting peak deflection is equivalent to the peak deflection in figure 14 b).

The peak deflection will be the superposition of the peak dynamic response plus the deflection at the same location due to the reciprocating lateral inertial load (0.127 MN) defined by the loading parameters. The displacement distribution at the natural frequency of the connecting rod is plotted in figure 14 b) for an acceleration amplitude of 13.2g which is required to achieve critical deflection.

The lateral deflection due to the reciprocating lateral inertial load has been calculated to be 0.313mm. Combining this value with the harmonic response yields a deflection of 2.188mm, which is in fact equivalent to the peak deflection due to the results of phase 1, as shown in figure 8 b).

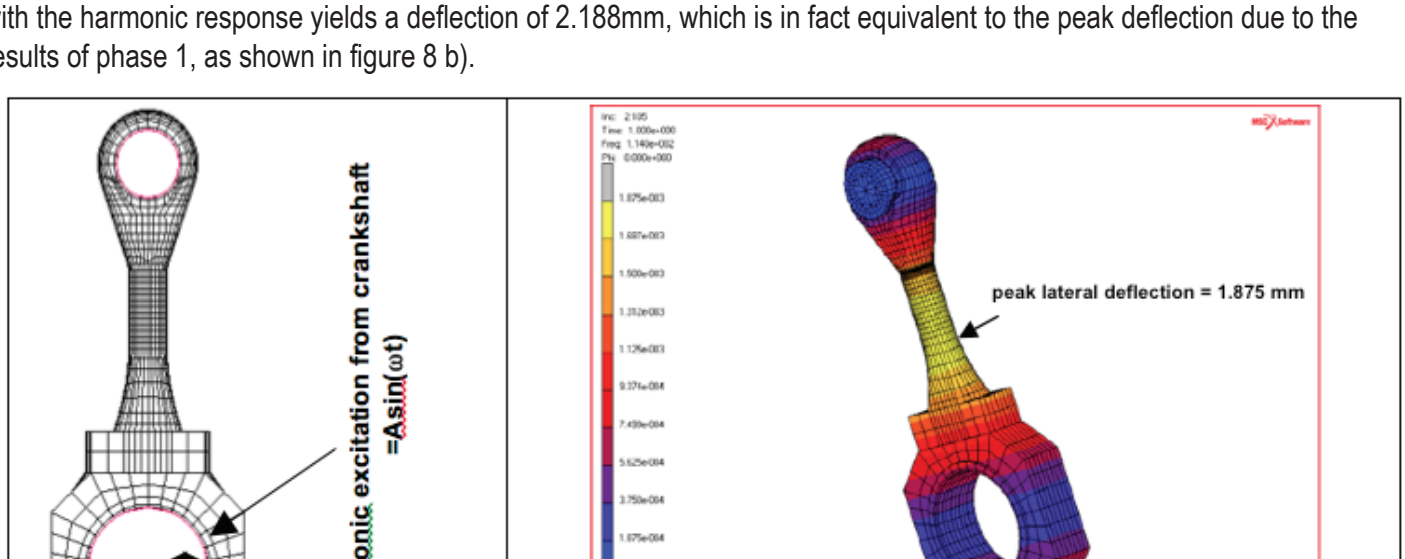

FIGURE 14. A) HARMONIC MODEL FOR CRANKSHAFT EXCITATION
B) ASSOCIATED LATERAL PEAK DEFLECTION DUE TO HARMONIC EXCITATION AT 13.2G

RESULTS:

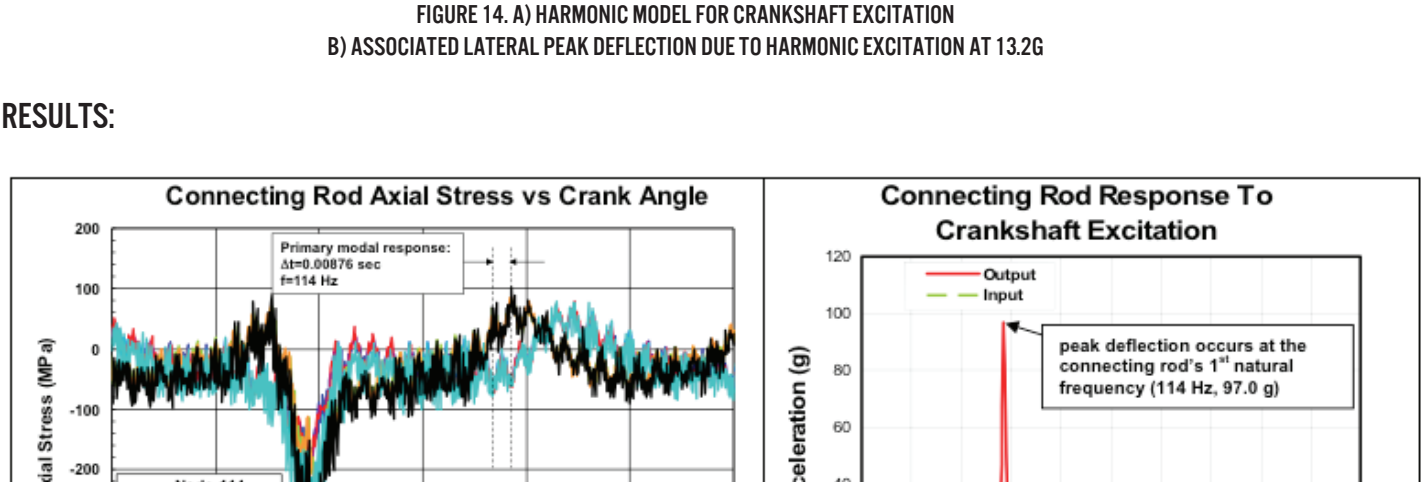

FIGURE 15. A) CONNECTING ROD AXIAL STRESS, 85% MILLER +8°ATDC
B) DYNAMIC ACCELERATION RESPONSE OF CONNECTING ROD WITH DAMPING = 1.0%

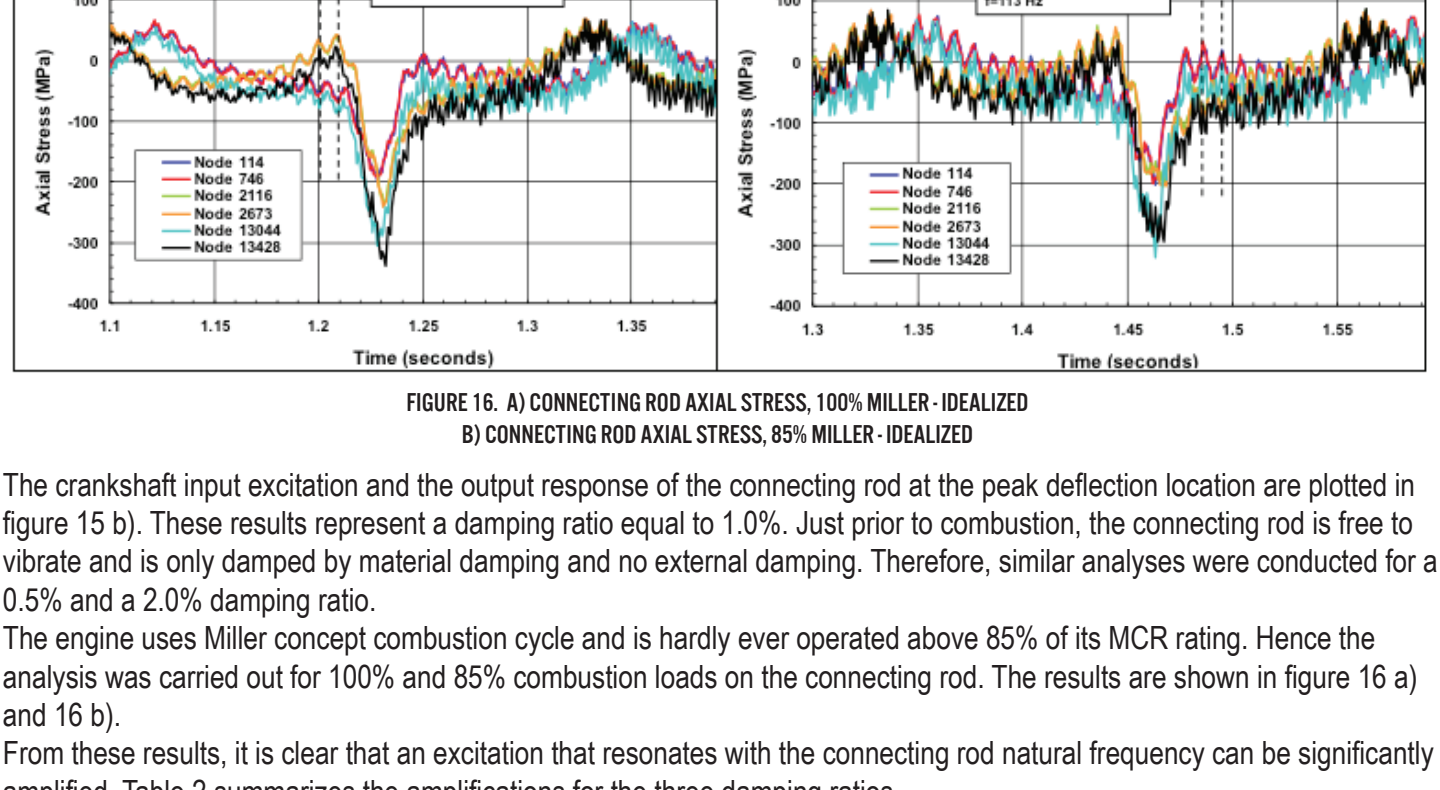

FIGURE 16. A) CONNECTING ROD AXIAL STRESS, 100% MILLER - IDEALIZED
B) CONNECTING ROD AXIAL STRESS, 85% MILLER - IDEALIZED

The crankshaft input excitation and the output response of the connecting rod at the peak deflection location are plotted in figure 15 b). These results represent a damping ratio equal to 1.0%. Just prior to combustion, the connecting rod is free to vibrate and is only damped by material damping and no external damping. Therefore, similar analyses were conducted for a 0.5% and a 2.0% damping ratio.

The engine uses Miller concept combustion cycle and is hardly ever operated above 85% of its MCR rating. Hence the analysis was carried out for 100% and 85% combustion loads on the connecting rod. The results are shown in figure 16 a) and 16 b).

From these results, it is clear that an excitation that resonates with the connecting rod natural frequency can be significantly amplified. Table 2 summarizes the amplifications for the three damping ratios.

TABLE 2. DYNAMIC AMPLIFICATION SUMMARY

Damping	Required harmonic excitation amplitude, A	Response amplification
0.5%	7.37 g	30.0
1.0%	13.2 g	16.7
2.0%	25.6 g	8.7

Based on the results of the analysis, fatigue diagrams were constructed for connecting rod. Figures 17 and 18 show fatigue diagrams for 100% idealized combustion cycle case and 100% Miller combustion cycle case respectively. As can be seen the connecting rod design is marginal to begin with and it exceeds the endurance limit with Miller cycle. Figure 19 shows the location where the connecting rod exceeds the endurance limit. The next step is to determine the torsional vibration of

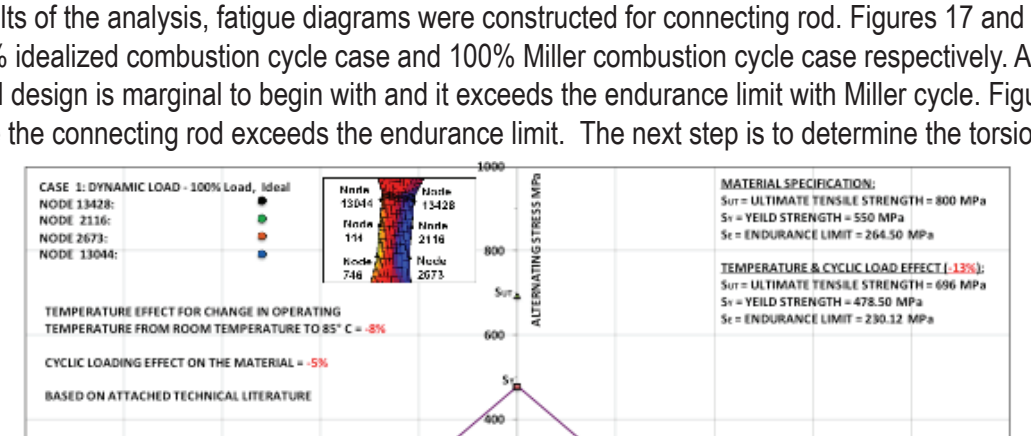

FIGURE 17. FATIGUE DIAGRAM DYNAMIC CALCULATIONS – 100% IDEALIZED ENGINE RATING

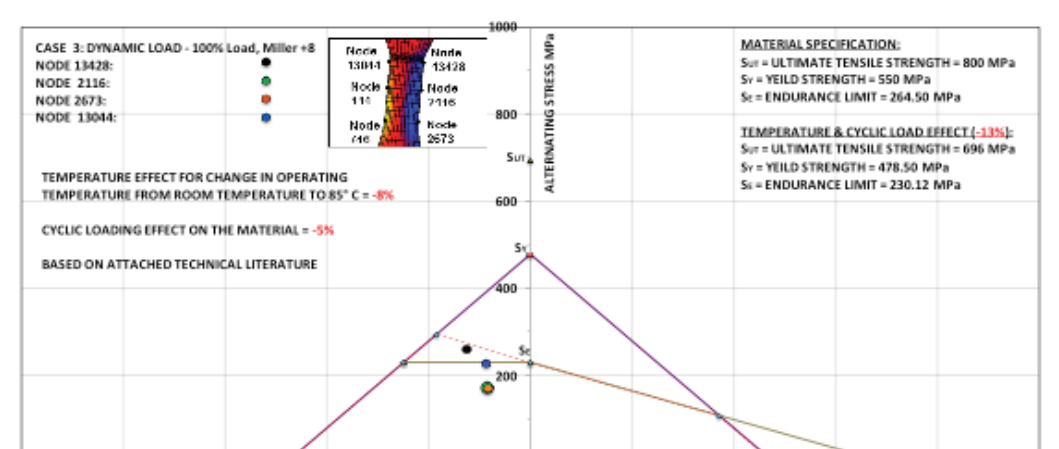

FIGURE 18. FATIGUE DIAGRAM DYNAMIC CALCULATIONS – 100% MILLER +8 ATDC

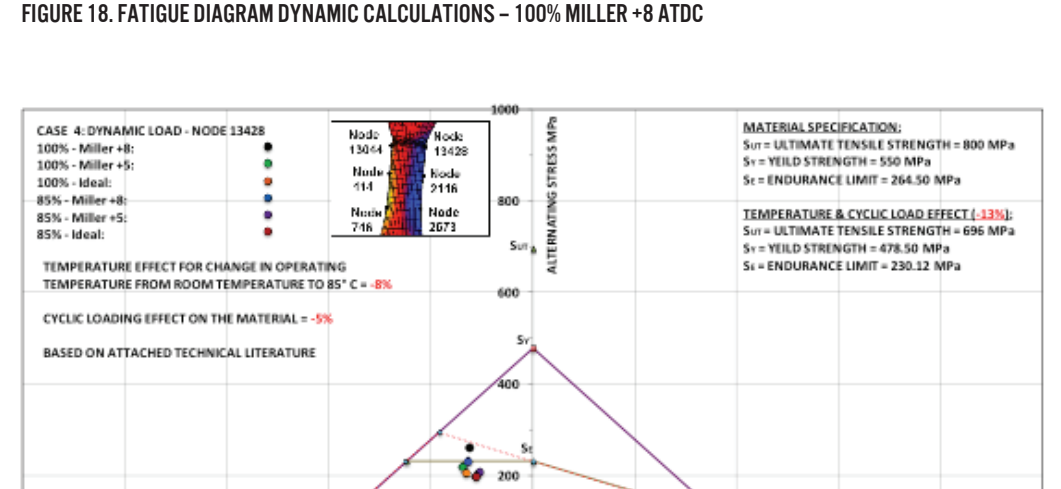

FIGURE 19. FATIGUE DIAGRAM DYNAMIC CALCULATIONS – NODE 13428

the crankshaft in terms of angular velocity and angular position and as a combination of the engine speed and the vibratory motion of the crankshaft as,

$$\omega = \omega_e + \beta \sin(\omega_c t) \qquad (5)$$

where is the engine's nominal speed, is the torsional vibration frequency of the crankshaft, and is the amplitude of the torsional vibratory angular velocity for the crankshaft. The angular motion is then defined as,

$$\theta = \int \omega dt = \omega_e t - \frac{\beta}{\omega_c} \cos(\omega_c t) \qquad (6)$$

$$\frac{d\theta}{dt} = \omega = \omega_e + \beta \sin(\omega_c t) \qquad (7)$$

$$\frac{d^2\theta}{dt^2} = \beta \omega_c \cos(\omega_c t) \qquad (8)$$

Near top dead center, the tangential motion (X-axis motion, u) is the driving excitation into the connecting rod. This motion can be defined in terms of the angular motion as,

$$u = r\sin(\theta) \quad \text{total displacement} \tag{9}$$

$$\frac{du}{dt} = r\cos(\theta)\frac{d\theta}{dt} \quad \text{total velocity} \tag{10}$$

$$\frac{d^2u}{dt^2} = r\left[-\sin(\theta)\left(\frac{d\theta}{dt}\right)^2 + \cos(\theta)\frac{d^2\theta}{dt^2}\right] \quad \text{total acceleration} \tag{11}$$

$$\frac{d^2u_e}{dt^2} = -r\omega_e^2\sin(\omega_e t) \quad \text{nominal engine speed contribution} \tag{12}$$

is the nominal engine speed contribution and r is the radial distance from the crankshaft axis to the crankshaft pin center. The total acceleration term, representing the tangential x-component of acceleration, includes the acceleration due to the engine speed. The engine speed contribution must be subtracted in order to obtain the oscillatory motion by itself. Therefore, the oscillatory tangential acceleration is defined as,

$$\frac{d^2u}{dt^2} = r\left[-\sin(\theta)\left(\frac{d\theta}{dt}\right)^2 + \cos(\theta)\frac{d^2\theta}{dt^2}\right] + r\omega_e^2\sin(\omega_e t) \quad \text{oscillatory acceleration} \tag{13}$$

For resonance condition, the vibratory motion of the crankshaft must be equal in frequency to that of the connecting rod such that =114 Hz. The amplitude ( ) of the crankshafts vibratory motion can then be determined by equating the maximum oscillatory tangential acceleration term to the crankshaft harmonic excitations listed in table 2 and solving for .In equation form, this becomes,

$$max\left(r\left[-\sin(\theta)\left(\frac{d\theta}{dt}\right)^2 + \cos(\theta)\frac{d^2\theta}{dt^2}\right] + r\omega_e^2\sin(\omega_e t)\right) = A \tag{14}$$

TABLE 3. OSCILLATION AMPLITUDES IN THE CRANKSHAFT MOTION

Damping	Angular velocity (β) (rad/sec)	Angular position (degrees)
0.5%	0.347	0.0277
1.0%	0.622	0.0497
2.0%	1.209	0.0968

Table 3 shows the resulting oscillations in angular velocity and position. These oscillation amplitudes cause yielding of the connecting rod and they have been shown not be detrimental to the structural integrity of the crankshaft. Table 4 shows calculated crankshaft stress amplitudes.

TABLE 4. VIBRATORY STRESS AMPLITUDE IN THE CRANKSHAFT (N/MM2)

Nodal point	Angular position 0.05 degrees (1% damping)	Angular position 0.1 degrees (2% damping)
1	18.1	36.3
2	17.7	35.5
3	17.3	34.6

FAILURE MODE:

We studied the failure mode by constructing a model of the complete crankshaft with the connecting rods, pistons, and cylinder liners as shown in Fig. 20 A. Some of the experts investigating the failure had argued that if the connecting rod was bent, it would shorten the connecting rod and that could have been easily detected. If the shortening of the connecting rod was not detected, then the connecting rod could not have been bent. So we carefully measured the minimum clearence of the connecting rod from the cylinder liner in an actual working engine. This was also used to verify the accuracy of our solid model as shown in Fig. 20 B. We followed it up with a finite element analysis for the collapse mode of the connecting rod. The collapse mode is represented graphically in Fig. 20 C. Fig. 20 D shows the damage caused to the engine block when the bent connecting rod hit the cylinder liner. The results of our finite element analysis were used to plot a curve of the connecting rod camber against the shoertening of the connecting rod as shown in Fig. 20 E. It can be clearly seen that connecting rod material reaches yeild point at 6.2 mm camber and it reached its ultimate tensile strength at 9.1 mm camber. Both these limits are reached well before the bent connecting rod will make contact with the cylinder liner (46 mm).

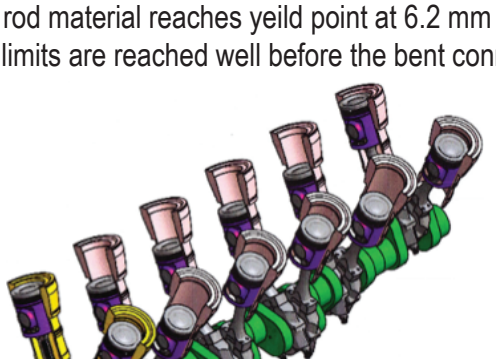

A. SOLID MODEL OF COMPLETE CRANKSHAFT WITH CONNECTING RODS, PISTONS, AND CYLINDER LINERS

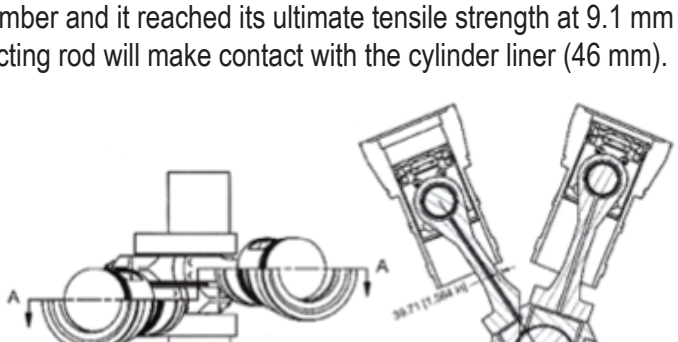

B. MINIMUM CLEARENCE BETWEEN THE CONNECTING ROD AND CYLINDER LINER IS APPROX. 40 MM

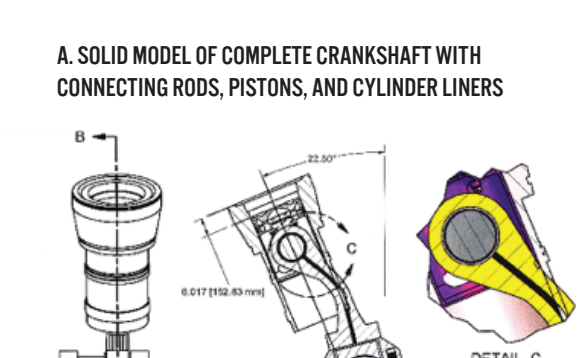

C. BENT CONNECTING ROD INTERFERING WITH AND DESTROYING THE CYLINDER LINER

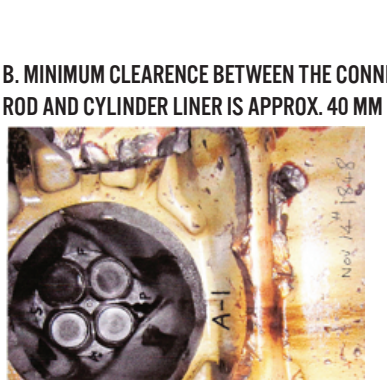

D. PICTURE OF THE ACTAUL ENGINE BLOCK DESTROYED BY THE CONNECTING ROD HITTING THE CYLINDER LINER

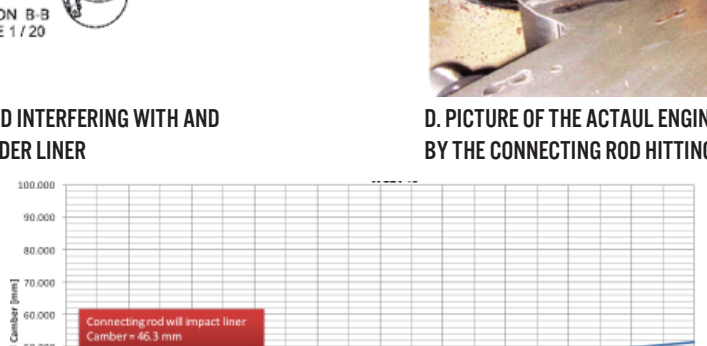

FIGURE 20. CONNECTING ROD FAILURE MODE STUDY MODEL AND CALCULATIONS

The interesting point is that when the bent connecting rod reaches its yeild and ultimate tensil strength points, the shortening in the length of connecting rod is 0.1 mm and 0.25 mm respectively. There is no way anyone can ever notice the shortened connecting rod. Even at the point of contact between the connecting rod and the cylinder liner, the shortening of the connecting rod is about 3.65 mm which is not something that would be easily noticeable.

PROPOSED SOLUTION:

Following an in-depth analysis of the connecting rod failures and testing several solutions for avoiding resonance with the crankshaft, the simplest solution was found to be redesigning the connecting rod and changing its natural frequency. The existing connecting rod was redesigned by increase in diameter of the shank and reduced length of the shank region by increasing the fillet radii. These changes produce a stiffer connecting rod with a higher section modulus. The results of modal analysis on the redesigned connecting rod shows a natural frequency of 137 Hz as shown in Fig. 21, which gives plenty of safety margin against resonance with the crankshaft. Fig. 22 shows the redesigned connecting rod with major dimensions. This solution is very beneficial for the system from a dynamic point of view but it is also a very expensive solution.

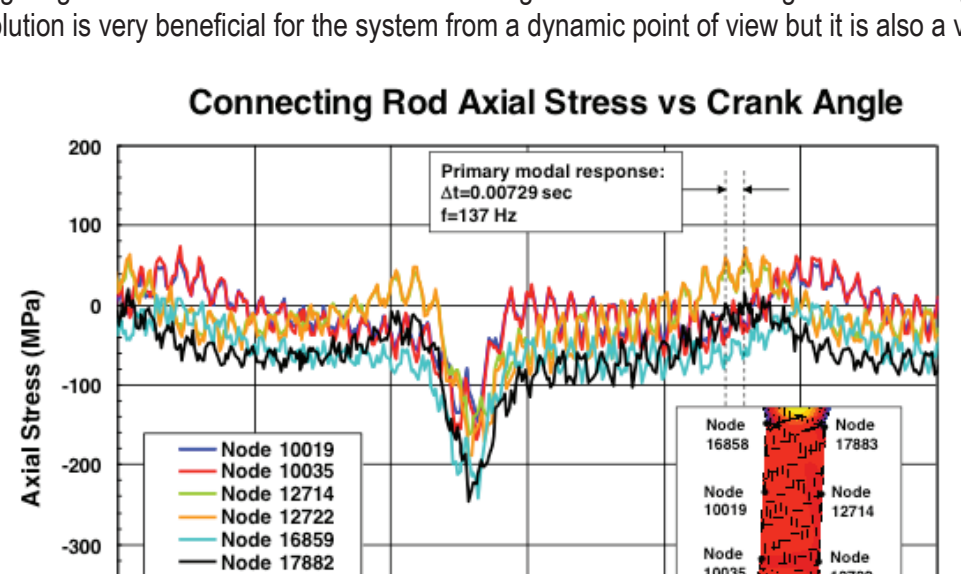

FIGURE 21. REDESIGNED CONNECTING ROD AXIAL STRESS, 100% MILLER +5 ATDC

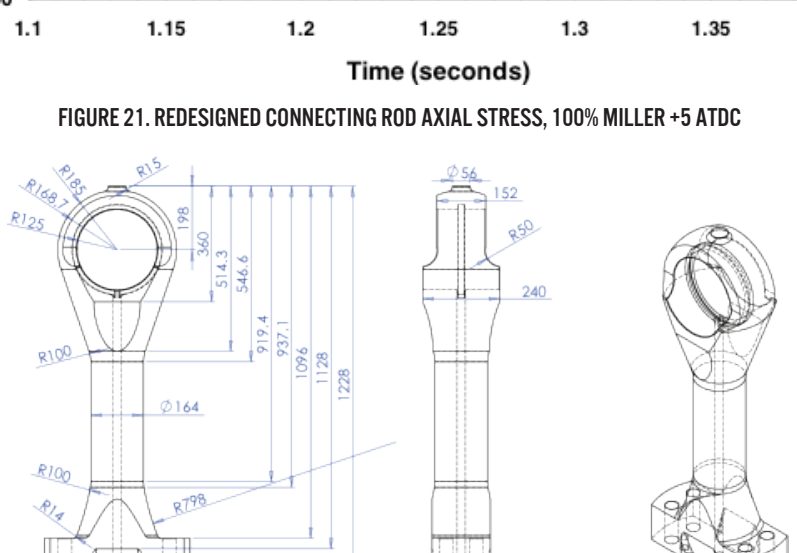

FIGURE 22. REDESIGNED CONNECTING ROD WITH MAJOR DIMENSIONS

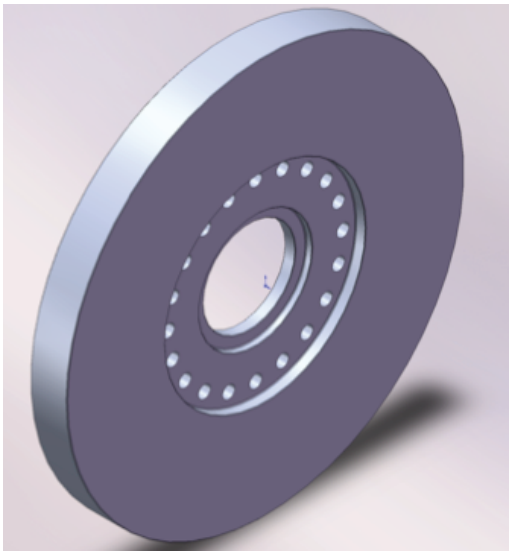

FIGURE 23. PROPOSED TUNING MASS

Another solution to this problem is adding a tuning mass to the crankshaft. This changes the natural frequency of the crankshaft and thereby helps in separating the dynamic response of the crankshaft from the connecting rod. This solution is much cheaper and easy to implement in existing systems. We designed a tuning mass as shown in Fig. 23, which will change the natural frequency of the crankshaft and drive it away from the connecting rod's horizontal first mode natural frequency.

DISCUSSIONS:

Torsional vibration modes in the crankshaft can resonate with the connecting rod's natural frequency. The resulting excitation can cause highly amplified bending in the connecting rod. This perturbation combined with the normal operating axial combustion forces are sufficient to cause local plastic deformation and lead to collapse of the connecting rod. Even if the collapse is not reached, elevated stresses are introduced which can lead to a significant reduction in fatigue life.

REFERENCES:

1. Wilson, C. E. and Sadler, P. J., 1993, "Kinematics and Dynamics of Machinery" 2nd edition, HarperCollins College Publishers.
2. Metallic Materials Properties Development and Standardization (MMPDS), page 2-28
3. Atlas Of Stress-Strain Curves. (n.d.). ASM International, 2nd Edition , 101.